Micromechanics of Hydride Formation and Cracking in Zirconium Alloys

J. Lufrano[1], **P. Sofronis**[1]

Abstract: Transient hydrogen diffusion and hydride formation coupled with material deformation are studied in Zr-2.5Nb alloys used in the pressure tubes of CANDU nuclear generating stations. The energetics of the hydride formation is revisited and the terminal solid solubility of hydrogen in solution is defined on the basis of the total elastoplastic work done on the system by the forming hydride and the external loads. Probabilistic precipitation of hydride is modeled in the neighborhood of a crack tip under mode I plane strain loading and a uniform initial hydrogen concentration below the stress free terminal solid solubility. Finite element analysis is used to monitor the local distribution and time evolution of hydrogen concentration, hydride volume fraction, stress, and strain as the externally applied loads increase. The mechanistic effects of the solute hydrogen and hydride formation on the stresses at the crack tip are analyzed and their consequence on the fracture toughness resistance of the material is determined.

keyword: plasticity, embrittlement, hydride, diffusion, hydrogen, fracture

1 Introduction

Hydrogen embrittlement, a severe degradation of the mechanical properties of materials in the presence of hydrogen, is governed by complex multiple mechanisms. Even in specific materials the embrittling mechanisms are not well established [Birnbaum and Sofronis (1994); Birnbaum, Robertson, Sofronis, and Teter (1997)]. One useful classification is to distinguish between systems which form hydrides and those which do not form hydrides under the relevant hydrogen fugacity and applied stress [Birnbaum (1984)].

A number of researchers [Birnbaum (1984); Birnbaum, Grossbeck, and Amano (1976); Takano and Suzuki (1974); Shih, Robertson, and Birnbaum (1988)] has shown that embrittlement in hydride forming materials occurs by hydride formation at severe stress raisers such as crack tips followed by cleavage of the brittle hydride [Westlake (1969)]. The phenomenon is intermittent, with the crack propagating through the hydride and stopping when it reaches the matrix. Subsequently, new hydride forms either autocatalytically [Shih, Robertson, and Birnbaum (1988)] or due to external loading, and then cleavage reinitiates [Westlake (1969)]. Stress induced hydride formation is a consequence of the volume dilatation, of the order of $\sim$15% which accompanies hydride precipitation [Birnbaum, Grossbeck, and Amano (1976); Westlake (1969); Gahr, Grossbeck, and Birnbaum (1977); Grossbeck and Birnbaum (1977); Flannagan, Mason, and Birnbaum (1981); Puls (1984)]. It has been experimentally shown [Gahr, Grossbeck, and Birnbaum (1977); Grossbeck and Birnbaum (1977)] that hydrides form in regions of hydrostatic tensile stress even at temperatures which are above the solvus temperature in the absence of stress. The hydride formation is a result of the enhanced hydrogen concentration in the area of tensile stress and the decreased chemical potential of the hydride relative to the solid solution in the same stress field [Birnbaum (1984); Gahr, Grossbeck, and Birnbaum (1977); Grossbeck and Birnbaum (1977); Flannagan, Mason, and Birnbaum (1981); Puls (1984)]. Mathematical modeling of these phenomena has been done by a number of authors [Dutton and Puls (1976); Dutton, Nuttall, Puls, and Simpson (1977); Ellyin and Wu (1994)]. Lufrano, Sofronis, and Birnbaum (1996) modeled the stress induced hydrogen transport and hydride formation in the vicinity of a stationary crack in an elastically accommodating matrix. Calculations were carried out to determine the effect of the hydrides on the stress field and the local stress intensity factor at the crack tip. In a subsequent work, Lufrano, Sofronis, and Birnbaum (1998) presented a detailed treatment of the plastic accommodation of hydrides and material elastoplasticity under load at a blunting crack tip in niobium.

In the present work, the kinetics of hydrogen diffusion and hydride formation in front of a blunting crack tip are studied in a zirconium alloy (Zr-2.5Nb). Calculations are carried out at room temperature of 25 C, and at temperatures of 250 and 310 C to simulate respectively the inlet and outlet temperature conditions prevailing at the pressure tubes of the CANDU nuclear reactor. Elastoplastic principles are used to calculate the total mechanical energy of hydride formation [Lufrano, Sofronis, and Birnbaum (1998)]. The calculations yield a point density of the hydride termed the "local hydride volume fraction", i.e., the probability of finding a hydride particle at a given location. Issues associated with hydride shape or the kinetics of the formation of an actual hydride particle are not addressed. Lastly, a Griffith fracture criterion based on the brittle cleavage of the formed hydride is proposed to assess the reduced fracture toughness observed in zirconium alloys in the presence of hydrogen.

[1] University of Illinois at Urbana-Champaign, Department of Theoretical and Applied Mechanics, 104 South Wright Street, Urbana, IL 61801, USA

2 Energy Changes in Hydride Formation

In the case of purely elastic accommodation, one by following Birnbaum, Grossbeck, and Amano (1976); Grossbeck and Birnbaum (1977); Gahr and Birnbaum (1978); Flannagan, Mason, and Birnbaum (1981); Puls (1981, 1984) can calculate the terminal solid solubility (TSS), namely the local solvus concentration c_s^σ measured in hydrogen atoms per solute atom in a material under external stress as [Lufrano, Sofronis, and Birnbaum (1996)]

$$c_s^\sigma = A \exp\left(\frac{H_h}{RT}\right) \exp\left(\frac{W_{\text{acc}}}{RT}\right) \exp\left(\frac{W_{\text{int}}}{RT}\right) \tag{1}$$

The parameter W_{acc} denotes the accommodation energy per mole of hydride formed in the absence of the external stress and W_{int} is the interaction energy of the formed hydride with the external stress, both of which are determined using elastic principles [Eshelby (1956, 1957)]. In Eq. 1, A is a constant determined experimentally, R is the gas constant, T is the absolute temperature, and H_h, which is negative, is the molal enthalpy change for transferring hydrogen from the solid solution to the hydride in the absence of any accommodation or any externally applied stress. However, since the volume increase associated with hydride formation in zirconium alloys is 17.1% [Puls (1981, 1984)], the metal deforms plastically to allow for the accommodation of the large volume change [Birnbaum, Grossbeck, and Amano (1976); Makenas and Birnbaum (1980); Birnbaum (1990)] and this plastic accommodation must be accounted for. In the absence of externally applied loads, Lee, Earmme, Aaronson, and Russell (1980); Earmme, Johnson, and Lee (1981) calculated the accommodation energy of a misfitting spherical precipitate assuming perfect plastic response. In a comprehensive study, Leitch and Puls (1992) used finite element techniques to calculate the accommodation energy of isotropically and anisotropically misfitting oblate spheroids in an elastic-perfectly plastic matrix. However, the validity of calculating the total energy of formation by using an elastoplastic accommodation energy along with an elastic interaction energy (cf. Eq. 1) is questionable.

Following Birnbaum, Grossbeck, and Amano (1976); Lufrano, Sofronis, and Birnbaum (1998), one can calculate the solvus concentration c_s^σ through

$$c_s^\sigma = B \exp\left(\Delta G_{\alpha-\beta}^{\text{tot}}/RT\right) \tag{2}$$

where B is an experimentally determined constant and $\Delta G_{\alpha-\beta}^{\text{tot}}$ is the Gibbs free energy change in forming a mole of hydride phase β from the solid solution phase α. The Gibbs free energy change can be generally written as

$$\Delta G_{\alpha-\beta}^{\text{tot}} = \Delta G_{\alpha-\beta}^{\text{chem}} + \Delta G_{\alpha-\beta}^{\text{sur}} + \Delta G_{\alpha-\beta}^{\text{mech}} \tag{3}$$

where $\Delta G_{\alpha-\beta}^{\text{chem}}$ is the chemical Gibbs energy change, $\Delta G_{\alpha-\beta}^{\text{sur}}$ is the free energy needed for the creation of the interface, and $\Delta G_{\alpha-\beta}^{\text{mech}}$ is the total mechanical free energy change in the hydride formation. For hydride formation with elastoplastic accommodation Birnbaum, Grossbeck, and Amano (1976) the free energy change is written as

$$\Delta G_{\alpha-\beta}^{\text{mech}} = \Delta G_{\alpha-\beta}^{\text{e}} + \Delta G_{\alpha-\beta}^{\text{p}} + \Delta G_{\alpha-\beta}^{\text{ext}} \tag{4}$$

where $\Delta G_{\alpha-\beta}^{\text{e}}$ is the elastic work done on the system (matrix+hydride) and is stored in the system as elastic energy, $\Delta G_{\alpha-\beta}^{\text{p}}$ is the plastic work dissipation, and $\Delta G_{\alpha-\beta}^{\text{ext}}$ is the work done by the external loads against the matrix displacement upon hydride formation. The change in elastic energy stored in the system, $\Delta G_{\alpha-\beta}^{\text{e}}$, can be evaluated with the use of

$$\Delta G_{\alpha-\beta}^{\text{e}} = \int_V \left(\int_t \sigma_{ij} D_{ij}^e \, dt \right) dV, \tag{5}$$

where σ_{ij} is the local Cauchy stress, D_{ij}^e is the elastic component of the deformation rate tensor (which equals the symmetric part of the velocity gradient in spatial coordinates), t is the time of formation, and V is the volume of the system (matrix+hydride). The plastic work done on the system $\Delta G_{\alpha-\beta}^{\text{p}}$ can be evaluated with the use of

$$\Delta G_{\alpha-\beta}^{\text{p}} = \int_V \left(\int_t \sigma_{ij} D_{ij}^p \, dt \right) dV, \tag{6}$$

where D_{ij}^p is the plastic component of the deformation rate tensor, and the work done by the external tractions $\Delta G_{\alpha-\beta}^{\text{ext}}$ can be evaluated with the use of

$$\Delta G_{\alpha-\beta}^{\text{ext}} = \int_S \left(\int_t T_i^{\text{ext}} v_i \, dt \right) dS, \tag{7}$$

where S is the surface bounding the volume V, T_i^{ext} is the component of the applied traction on S, and v_i is the component of the surface velocity. It is worth mentioning here that the elastic formulation expressed in Eq. 1 can be viewed as a special case of the more general elastoplastic formulation expressed in Eqs. 2 and 3 by setting $\Delta G_{\alpha-\beta}^{\text{mech}} = \Delta G_{\alpha-\beta}^{\text{acc}} + \Delta G_{\alpha-\beta}^{\text{int}}$.

Since zirconium alloys undergo plastic deformation to allow for the accommodation of hydride Puls (1978, 1981, 1984, 1990); Leitch and Puls (1992) the terminal solid solubility is not an "equilibrium" value for the solute hydrogen concentration in contact with the hydride phase. The chemical and surface energy terms of Eq. 3 represent thermodynamically reversible processes such that $\Delta G_{\alpha-\beta}^{\text{chem}} = -\Delta G_{\beta-\alpha}^{\text{chem}}$ and $\Delta G_{\alpha-\beta}^{\text{sur}} = -\Delta G_{\beta-\alpha}^{\text{sur}}$ [Birnbaum, Grossbeck, and Amano (1976)]. However, due to the plastic accommodation of the matrix, a complete cycle of hydride formation and dissolution results in lost energy in the form of thermally dissipated plastic work. Thus, in general, $\Delta G_{\alpha-\beta}^{\text{mech}} \neq -\Delta G_{\beta-\alpha}^{\text{mech}}$ and, as such, $\Delta G_{\alpha-\beta}^{\text{tot}} \neq -\Delta G_{\beta-\alpha}^{\text{tot}}$. However, dissolution of the hydride upon unloading is not taken into account in the present study.

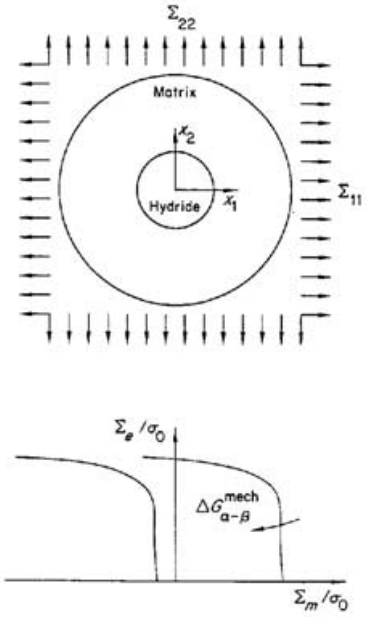

Figure 1 : The system in plane strain deformation and a representation for the contour plots of the total mechanical energy of hydride formation $\Delta G^{\text{mech}}_{\alpha-\beta}$ in stress space (elastoplastic matrix response) [Lufrano, Sofronis, and Birnbaum (1998)].

Numerical calculations were carried out to estimate the total mechanical energy of formation of a hydride precipitate with an isotropic linearly elastic response in an infinite zirconium matrix with an isotropic linearly elastic, perfectly plastic response under plane strain conditions. The elastoplastic response of the matrix material requires the hydride precipitation to be modeled in an incremental fashion. It was assumed that the entire volume of the precipitate uniformly acquires the transformation strain that accompanies hydride formation. External forces were applied so that the entire range of stress space was spanned.

In accordance with the plane strain assumption in the model, the precipitating hydride particle and the zirconium alloy matrix were modeled as circular cylinders, as seen in Fig. 1 [Lufrano, Sofronis, and Birnbaum (1998)]. There was no diffusion of hydrogen in this part of the calculation. While it is known that the transformation strain is anisotropic [Somenkov (1972); Suzuki (1985); Puls (1981)], the largest stress contributions to the hydride free energies arise from the dilatational component. Thus, in the context of the large strain formulation, the deformation rate due to the hydride is phrased as

$$D^T_{ij} = \frac{d}{dt}\left[\ln\left(1+\frac{1}{3}e^T\right)\right]\delta_{ij} \tag{8}$$

where d/dt denotes differentiation with respect to time, e^T is the dilatational transformation strain (equal to θ_{hyd} which is the volume dilatation of a material element that is 100% hydride), and δ_{ij} is the Kronecker delta.

For finite deformations, the associated flow rule for von Mises yielding and perfect plasticity is given by the classical Prandtl—Reuss equations appropriately modified to account for transformation induced strain in the lattice:

$$\overset{\nabla}{\sigma}_{ij} = 2G\left[\delta_{ik}\delta_{jl} + \frac{\nu}{1-\nu}\delta_{ij}\delta_{kl} - \frac{3}{2}\frac{\sigma'_{ij}\sigma'_{kl}}{\sigma_0^2}\right]\left(D_{kl} - D^T_{kl}\right) \tag{9}$$

for plastic loading and

$$\overset{\nabla}{\sigma}_{ij} = 2G\left(\delta_{ik}\delta_{jl} + \frac{\nu}{1-\nu}\delta_{ij}\delta_{kl}\right)\left(D_{kl} - D^T_{kl}\right) \tag{10}$$

for elastic loading or any unloading, where D_{ij} is the deformation rate tensor, the superposed ∇ denotes the Jaumann or co-rotational stress rate (which exhibits proper material invariance for rigid spin), $\sigma'_{ij} = \sigma_{ij} - \sigma_{kk}\delta_{ij}/3$ is the deviatoric stress, σ_0 is the yield stress, and G and ν are the shear modulus and Poisson's ratio respectively. Thus the constitutive equation of the elastically deforming hydride cylinder (see Fig. 1) is given by Eqs. 8 and 10, whereas the constitutive equation of the surrounding elastoplastically deforming niobium cylinder is given by Eqs. 9 and 10 with D^T_{ij} set equal to zero.

The governing equations for the rate equilibrium accounting for changes of the deformed volume of the material are cited by McMeeking and Rice (1975) as

$$\int_V \left(\overset{\nabla}{\sigma}_{ij} + D_{kk}\sigma_{ij}\right)\delta D_{ij}\,dV - \int_V \frac{1}{2}\sigma_{ij}\delta\left(2D_{ik}D_{kj} - v_{k,i}v_{k,i}\right)dV = \int_S \dot{T}_i\delta V_i\,dS \tag{11}$$

where a superposed dot denotes time differentiation, T_i is the traction (which is equal to T^{ext}_i on the part of the surface where tractions are prescribed), and δ indicates an arbitrary virtual variation of the quantity it precedes. Any virtual variation of the velocity is constrained to vanish on the part of the surface where velocities are prescribed. The finite element equations were derived from the variational statement (11), and were modified to allow for nearly incompressible material response [Nagtegaal, Parks, and Rice (1974)]. The constitutive equations (9) and (10) were integrated by using the backward Euler integration technique [Lufrano (1996)]. The formulation of Govindarajan and Aravas (1994) for large strain plasticity was adopted to ensure zero lattice strain during large rigid body rotation.

All material constants used in this investigation were for the irradiated material [Puls (1990)]. Young's modulus and Poisson's ratio for both the hydride and the matrix were given as function of temperature respectively by $E = 95.9 - 0.0574(T-273)\ GPa$ and $\nu = 0.436 - 4.8\times10^{-6}(T-300)$. The flow stress dependence on temperature was given by $\sigma_0 = (1388 - 1.02T)\ MPa$. The volume dilatation upon hydride formation was $\theta_{\text{hyd}} = 17.1\%$ with a partial molar volume of the

Table 1 : Material parameters for irradiated Zr-2.5%Nb at room, inlet pressure tube, and outlet pressure tube temperatures.

$T\ (K)$	$E\ (GPa)$	ν	$\sigma_0\ (MPa)$	$D\ (m^2/s)$
298	94.5	0.436	1084	1.54×10^{-13}
523	81.6	0.329	854	6.79×10^{-11}
583	78.1	0.300	793	1.56×10^{-10}

Table 2 : Energy changes in hydride formation at room, inlet pressure tube, and outlet pressure tube temperatures.

T (K)	$\Delta G^{\text{mech}}_{\alpha-\beta}\Big\vert_{\Sigma_m=0,\Sigma_e=0}$ $(kJ/mole)$	$\Delta G^{\text{chem}}_{\alpha-\beta} + \Delta G^{\text{sur}}_{\alpha-\beta}$ $(kJ/mole)$
298	6.308	-35.250
523	4.765	-35.707
583	4.313	-33.255

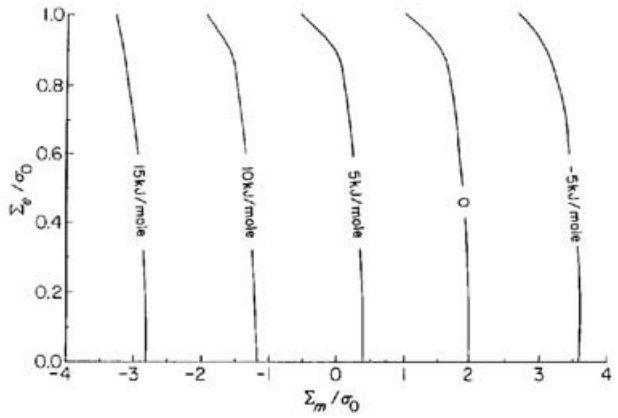

Figure 2 : Contour plots in stress space of the total mechanical energy of hydride formation $\Delta G^{\text{mech}}_{\alpha-\beta}$ at temperature of 298 K.

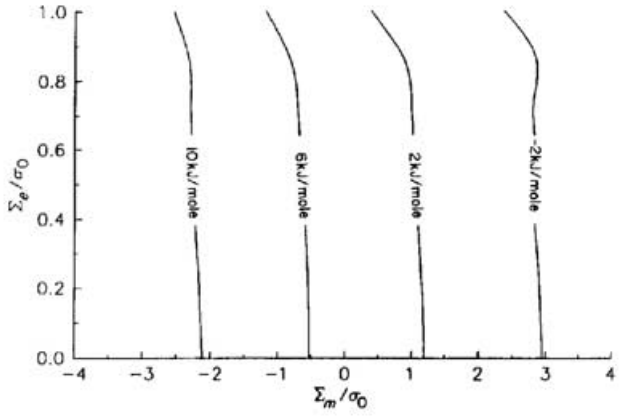

Figure 3 : Contour plots in stress space of the total mechanical energy of hydride formation $\Delta G^{\text{mech}}_{\alpha-\beta}$ at temperature of 523 K.

hydride $V_{\text{HYD}} = 16.3 \times 10^{-6}\, m^3/mole$. The molar volume V_M of the host lattice equaled $13.85 \times 10^{-6}\, m^3/mole$. The values of the elastic moduli, yield stress and diffusion coefficient at the three temperatures of interest, namely 25 C, 50 C and 310 C, are displayed on Tab. 1.

At ratios of the radius of the matrix to the radius of the precipitate of greater than 20 to 1, the size effects of the matrix were negligible. Tractions $T_i^{\text{ext}} = \Sigma_{ij} n_j$ on the external surface S with outward unit normal n_i were applied all around to control the macroscopic state of stress Σ_{ij} in the composite material (see Fig. 1). The macroscopic stress Σ_{ij} can be described by the macroscopic hydrostatic component $\Sigma_m = \Sigma_{kk}/3$ and the deviatoric component $\Sigma_e = \sqrt{3\Sigma'_{ij}\Sigma'_{ij}/3}$ where $\Sigma'_{ij} = \Sigma_{ij} - \Sigma_{kk}\delta_{ij}/3$. To span the range of possible values of plane strain stress space for a perfectly plastic material, it is sufficient to let the normalized macroscopic hydrostatic stress Σ_m/σ_0 vary between -4.0 and 4.0 and to let the normalized macroscopic deviatoric stress Σ_e/σ_0 vary between zero and one.

Contour plots for the total mechanical energy of formation per mole of precipitated hydride are displayed in Figs. 2-4 at temperatures 25, 250 and 310 C respectively. The corresponding elastoplastic accommodation energies, i.e. $\Delta G^{\text{mech}}_{\alpha-\beta}$ in the absence of external loads, are 6.308, 4.765 and 4.313 $kJ/mole$ (Tab. 2). The decrease in the elastoplastic accommodation energy of formation with increasing temperature is consistent with the accompanying material softening. As seen in the Figs. 2-4, at low levels of deviatoric stress, e.g. $\Sigma_e/\sigma_0 \leq 0.8$, the total mechanical energy exhibits a minimal dependence on the macroscopic deviatoric stress Σ_e/σ_0. However, at a given hydrostatic stress and higher levels of deviatoric stress, e.g. $\Sigma_e/\sigma_0 > 0.8$, the total mechanical energy of formation begins to decrease markedly as the macroscopic deviatoric stress increases, with the largest rate of decrease occurring as the matrix material approaches yield, i.e. $\Sigma_e/\sigma_0 = 1.0$.

3 Elastoplastic Calculation of the Terminal Solid Solubility

Experimental measurements [Puls (1990); Shi, Shek, and Puls (1995)] of the stress-free solvus yield

$$c_s^0 = 10.32 \exp\left(\frac{-28.942 kj/mole}{RT}\right) \tag{12}$$

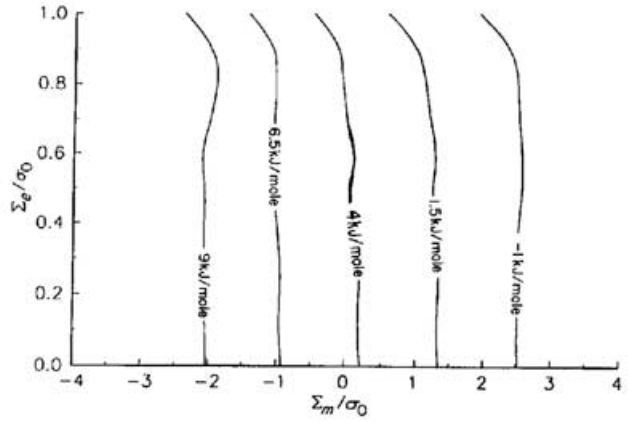

Figure 4 : Contour plots in stress space of the total mechanical energy of hydride formation $\Delta G^{\text{mech}}_{\alpha-\beta}$ at temperature of 583 K.

which when combined with Eqs. 2 and 3 provides

$$\Delta G^{\text{chem}}_{\alpha-\beta} + \Delta G^{\text{sur}}_{\alpha-\beta} + \Delta G^{\text{mech}}_{\alpha-\beta}\Big|_{\Sigma_m=0,\Sigma_e=0} = -28.942 \quad kJ/mole \tag{13}$$

Using the elastoplastic accommodation energy $\Delta G^{\text{mech}}_{\alpha-\beta}\Big|_{\Sigma_m=0,\Sigma_e=0}$ as calculated in Section 2, one can then calculate from Eq. 3 the sum $\Delta G^{\text{chem}}_{\alpha-\beta} + \Delta G^{\text{sur}}_{\alpha-\beta}$. The corresponding values for the three temperatures of interest are shown at Tab. 2. Substitution of these values for $\Delta G^{\text{chem}}_{\alpha-\beta} + \Delta G^{\text{sur}}_{\alpha-\beta}$ in Eqs. 2 and 3 yields the solvus concentration for any level of externally applied stress as

$$c_s^{\sigma} = 10.32 \exp\left(\frac{-35.250\, kJ/mole}{RT}\right) \exp\left(\frac{\Delta G^{\text{mech}}_{\alpha-\beta}}{RT}\right) \quad \text{at } T = 298\, K, \tag{14}$$

$$c_s^{\sigma} = 10.32 \exp\left(\frac{-33.707\, kJ/mole}{RT}\right) \exp\left(\frac{\Delta G^{\text{mech}}_{\alpha-\beta}}{RT}\right) \quad \text{at } T = 523\, K, \tag{15}$$

$$c_s^{\sigma} = 10.32 \exp\left(\frac{-33.255\, kJ/mole}{RT}\right) \exp\left(\frac{\Delta G^{\text{mech}}_{\alpha-\beta}}{RT}\right) \quad \text{at } T = 583\, K. \tag{16}$$

The total mechanical energy of formation to be used in Eqs. 14-16 is extrapolated from Figs. 2-4 correspondingly. At a given hydrostatic stress and at high levels of deviatoric stress, e.g. $\Sigma_e/\sigma_0 > 0.8$, the value of $\Delta G^{\text{mech}}_{\alpha-\beta}$ required to match the experimental solvus is markedly less than the $\Delta G^{\text{acc}}_{\alpha-\beta} + \Delta G^{\text{int}}_{\alpha-\beta}$ required by the elastic formulation as given by Eq. 1.

4 Governing Equations for Hydrogen Diffusion Accounting for Hydride Formation Coupled with Material Elastoplastic Deformation

4.1 Formulation of the hydrogen diffusion initial boundary value problem allowing for hydride formation

Modeling of stress driven transient diffusion of hydrogen and the corresponding formulation of the initial boundary value problem follow the methodology developed by Lufrano, Sofronis, and Birnbaum (1996, 1998) The hydrogen diffusion constant [Puls (1990)] in zirconium alloys is given by $D = 2.17 \times 10^{-7} \exp(-35.1\, kJ/mole/RT)\ m^2/s$, (see Tab. 1), and the activation energy for hydrogen diffusion through hydride was taken to be equal to three times the activation energy for diffusion through the solid solution phase [Völkl and Alefeld (1978)]. Hence, in the present study, the dominant mode for diffusion is through the solid solution. To model the conditions representing internal embrittlement, a zero hydrogen flux boundary condition was used.

Let C_L denote the hydrogen concentration in the lattice expressed as hydrogen atoms per unit volume of solid solution phase when the hydride volume fraction f is less than 1. At a given time with the composition of the composite defined pointwise by its hydride volume fraction f such that $0 \le f \le 1$, the hydrogen diffusion equation [Lufrano, Sofronis, and Birnbaum (1996)] is written as follows:

$$Q\frac{\partial C_L}{\partial t} = \left(D_c C_{L,i} + \frac{D_c C_L}{RT}\mu_{\sigma,i}\right)_{,i} \tag{17}$$

where $()_{,i} = \partial()/\partial x_i$, Q is given as

$$Q = \begin{cases} 1-f & \text{if} \quad 0 \le f < 1 \\ 1 & \text{if} \quad f = 1 \end{cases}, \tag{18}$$

D_c is an effective diffusion constant for the hydrogen diffusing through the composite material given by

$$D_c = \begin{cases} (1-f)D & \text{if} \quad 0 \le f < 1 \\ D_h & \text{if} \quad f = 1 \end{cases}, \tag{19}$$

where D and D_h represent the diffusion constants of hydrogen in solution with metal and in the hydride respectively. The parameter μ_σ is the stress dependent part of the chemical potential of hydrogen in solution and is given by $\mu_\sigma - \mu_0 = -\sigma_{kk}V_H/3$, where μ_0 is the chemical potential in the unstressed volume and only dilatational distortion of the lattice is considered. The partial molar volume of hydrogen V_H in solution is equal to $1.67 \times 10^{-6}\ m^3/mole$ [Puls (1990)]. It should be mentioned that μ_σ as used in Eq. 17 was also used to represent the effect of stress on the chemical potential of the hydrogen in the hydride which is in equilibrium with the solid solution. A forward Euler solution procedure was used to solve Eq. 17 incrementally in time at given hydride volume fraction. At the end of each increment, the lever rule was used to determine

the additional amount of hydride formed if the local hydrogen concentration was calculated to be greater than the local solvus concentration as determined by Eqs. 14-16. The relevant methodology can be found in the work by Lufrano, Sofronis, and Birnbaum (1996)

4.2 *Formulation of the elastoplasticity boundary value problem*

Formulation of the large strain elastoplastic boundary value problem follows the methodology outlined in Section 2. The composite material (matrix+hydride) is taken to have an elastoplastic response characterized by Eqs. 9 and 10 in which the deformation rate tensor D^T_{ij} for the volume dilatation due to interstitial hydrogen in solution and hydride formation is given by Eq. 8, where e^T is now given by

$$e^T = \begin{cases} (c-c_0)\theta_h & \text{if} \quad f=0 \\ (1-f)(c-c_0)\theta_h + f(\theta_{\rm hyd} - c_0\theta_h) & \text{if} \quad f\neq 0 \end{cases} \tag{20}$$

In Eq. 20, c and c_0 are the local and initial hydrogen concentration in hydrogen atoms per metal atom respectively (H/M), and θ_h is the lattice local dilatation when a hydrogen atom dissolves in solution with the metal [Peisl (1978)] and is calculated from the partial molar volume of hydrogen in solution. The yield stress σ_0 was assumed to be independent of the local hydrogen concentration and hydride volume fraction.

4.3 *Hydrogen transport and small scale hydride formation at a blunting crack tip*

Modeling was carried out under the assumption of small scale yielding and hydride formation conditions, with the initial conditions of a uniform initial concentration c_0 below the stress free terminal solid solubility (see Tab. 3), and f and $\dot{f}$ set equal to zero at $t=0$. For the temperatures of interest, Tab. 3 shows the initial concentrations used in the calculations along with the corresponding stress free solvus concentrations, calculated by Eqs. 14-16 with the value of $\Delta G^{\rm mech}_{\alpha-\beta}$ taken from Tab. 2. As will be shown later, the stress induced formation of hydride results in local stress relaxation, raising the possibility of hydride dissolution. In view of the plastic accommodation and resulting hysteresis, dissolution of hydride was not modeled. In all of the numerical experiments, the crack was loaded under plane strain mode I conditions at a constant displacement rate during a loading time $t_1 = 3600\ s$, at the end of which the final load phrased in terms of the applied stress intensity factor was $K_A = 20\ MPa\sqrt{m}$. At times t_e greater than t_1 the loading displacements were held fixed. The solution methodology to the transient hydrogen diffusion initial value problem coupled to the large strain elastoplasticity boundary value problem is described in the work by Lufrano, Sofronis, and Birnbaum (1996, 1998).

Table 3 : Values of the initial concentration c_0 and stress free solvus c_s^0 used in the calculations at room, inlet pressure tube, and outlet pressure tube temperatures.

$T\ (K)$	$c_0\ (H/M)$	$c_s^0\ (H/M)$
298	1.0×10^{-5}, 4.0×10^{-5}	8.77×10^{-5}
523	0.003, 0.010	0.0133
583	0.01	0.0264

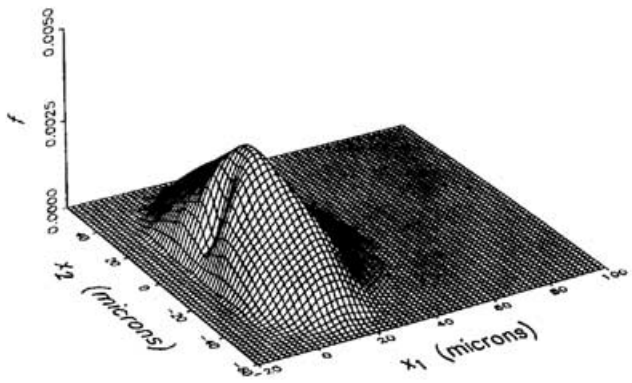

Figure 5 : Surface plot of the hydride volume fraction f in the region in front of a blunted crack after an elapsed time of 2 years. The load time was $t_l = 3600$ seconds, $K_A = 20\ MPa\sqrt{m}$, the initial concentration 0.00001 H/M, and the temperature 298 K.

5 Numerical Results

A total of 939 four-noded quadrilateral isoparametric finite elements with 1007 nodes [Sofronis and McMeeking (1989)] was used in the calculations. The distance from the crack tip to the outer boundary was set to equal to 10 cm. Through fine discretization of the near tip area, it was ensured that hydride formation took place in a region which contained 25 radial zones of finite elements centered at the crack tip. Numerical experiments carried out with a larger number of zones in the same region yielded identical results.

5.1 *Room temperature ($T = 298\ K$)*

Finite element calculations were carried out with an initial hydrogen concentration $c_0 = 0.00001\ H/M$ which was much less than the stress free solvus of 0.0000877 H/M. Fig. 5 shows a surface plot of the hydride volume fraction f plotted in the region in front of a blunted crack after the application of the external load of $K_A = 20\ MPa\sqrt{m}$ in time $t_1 = 3600\ s$ and after a total elapsed time t_e of 2 years. Fig. 6 shows the hydride volume fraction f in front of the blunting crack tip subjected to an applied load of K_A in load time t_l plotted against the dis-

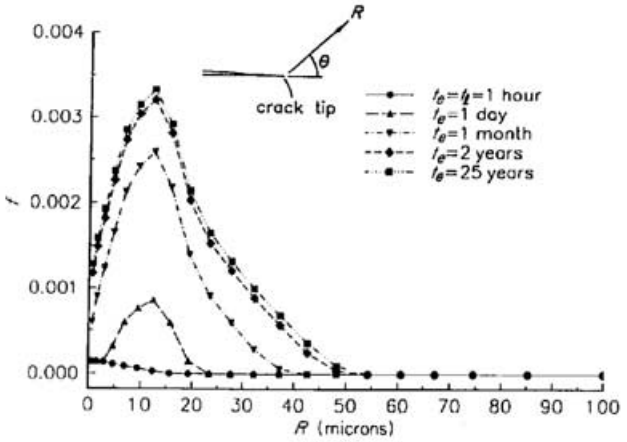

Figure 6 : Plot of the hydride volume fraction f versus distance R ahead of the crack tip at $\theta = 0$ after total elapsed times $t_e = 1$ hour, 1 day, 1 month, 2 years and 25 years. The load time was $t_l = 3600$ seconds, $K_A = 20\, MPa\sqrt{m}$, the initial concentration 0.0001 H/M and the temperature 298 K.

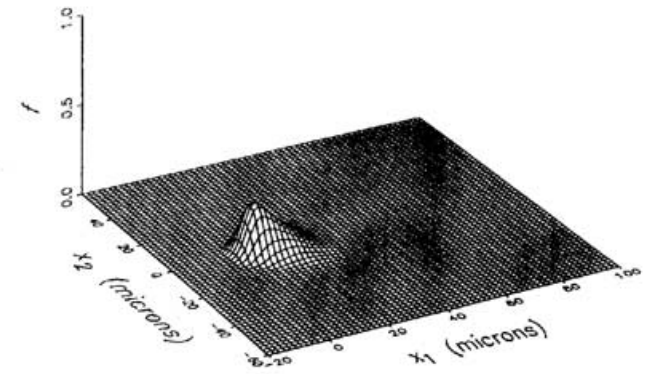

Figure 7 : Surface plot of the hydride volume fraction f in the region in front of a blunted crack after the completion of loading ($K_A = 20\, MPa\sqrt{m}$). The load time was $t_l = 3600$ seconds, the initial concentration 0.003 H/M, and the temperature 523 K .

tance from the crack tip R, at $\theta = 0$ for total elapsed times of 1 hour, 1 day, 1 month, 2 years and 25 years. The peak in the local hydride volume fraction occurs approximately 10 – 15 microns in front of the crack tip instead of directly at the crack tip due to the character of the crack tip stress field in the case of elastoplastic blunting. Fig. 6 shows continued hydride growth after the loading has been completed at time $t_l = 3600$ s. Also of note is that the hydride zone has a definite shape that is not identified with the contours of equal hydrostatic stress ahead of the crack tip. This is a result of the effect of the deviatoric stresses near yield on the elastoplastic energy of formation, which specifically results in a significant lowering of the energy of formation and hence a lowering of the solvus concentration. It should be noted that this result is a direct consequence of the consideration of elastoplastic energy of hydride formation, and accordingly it is not predicted under the assumption of entirely elastic accommodation of the hydride formation [Lufrano, Sofronis, and Birnbaum (1996)]. Similar behavior, but with larger hydride volume fractions (less than 0.9% though), was observed in the calculations carried out at a higher initial concentration, $c_0 = 0.00004\, H/M$ [Lufrano and Sofronis (1998)].

Figs. 5 and 6 demonstrate clearly that at room temperature the amounts of hydride formed ahead of a crack are not substantial ($f \sim 0.1\%$) for initial concentrations of hydrogen much less than the stress free solvus. As a result, no significant effect due to the local volume dilatation is observed on the stress state in the immediate crack tip neighborhood. Furthermore, equilibrium of the local hydride with the local stress is not reached even after 2 years from the application of the load (Fig. 6). This is attributed to the synergistic effect of the relatively small initial concentration in the system and the slow diffusivity of hydrogen in the zircalloy when compared with other systems, such as niobium [Lufrano, Sofronis, and Birnbaum (1996, 1998)].

5.2 Pressure tube inlet temperature ($T = 523K$)

At an initial hydrogen concentration $c_0 = 0.003\, H/M$ (stress free solvus $c_s^0 = 0.0133\, H/M$), Figs. 7 and 8 show surface plots of the hydride volume fraction f plotted in the region in front of the blunted crack after the application of the external load of $K_A = 20\, MPa\sqrt{m}$ and after a total elapsed time t_e of 1 hour and 1 month respectively. Fig. 9 shows the hydride volume fraction f in front of the blunting crack tip subjected to $K_A = 20\, MPa\sqrt{m}$ plotted against the distance from the crack tip R, at $\theta = 0$, for total elapsed times of 1 hour, 1 day, 1 month, 2 years and 25 years. Autocatalytic hydride growth is observed under constant load as at room temperature, but now hydride reaches equilibrium with local stress approximately in a month. In contrast with the room temperature case, the higher initial concentration used in the present calculation in combination with the higher hydrogen diffusivity at $T = 523\ K$ yields larger amounts, of order ∼10%, of hydride volume fractions at the tip (Fig. 9). As a result, a continued stress relaxation occurs in conjunction with the post-loading autocatalytic hydride growth. The effect is shown in Fig. 10 in which the normalized normal stress σ_{22}/σ_0 is plotted in front of the blunted crack tip against the distance from the crack tip R at $\theta = 0$, for total elapsed times of 1 hour, 1 day, 1 month, 2 years and 25 years. For reference purposes the normalized normal stress, σ_{22}/σ_0, from a hydrogen-free sample is also plotted in the Figure. A ∼20% percent reduction

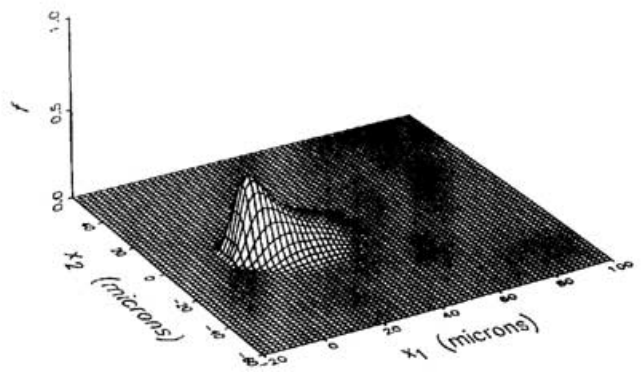

Figure 8 : Surface plot of the hydride volume fraction f in the region in front of a blunted crack after an elapsed time of 1 month. The load time was $t_l = 3600$ seconds, $K_A = 20$ $MPa\sqrt{m}$, the initial concentration 0.003 H/M, and the temperature 523 K.

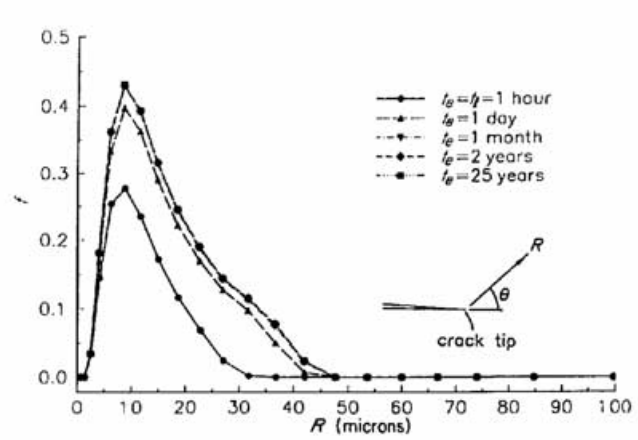

Figure 9 : Plot of the hydride volume fraction f versus distance R ahead of the crack tip at after total elapsed times $t_e = 1$ hour, 1 day, 1 month, 2 years and 25 years. The load time was $t_l = 3600$ seconds, $K_A = 20$ $MPa\sqrt{m}$, the initial concentration 0.003 H/M and the temperature 523 K.

in the peak normal stress in front of the crack tip occurs after a total elapsed time of 1 month when equilibrium conditions have almost been reached.

Faster and more drastic hydride precipitation was observed when an initial hydrogen concentration of $c_0 = 0.01$ H/M was used in the simulations [Lufrano and Sofronis (1998)]. The plot of the hydride volume fraction against the distance from the crack tip R at $\theta = 0$ for total elapsed times of 1 hour, 1 day, 1 month, 2 years and 25 years (Fig. 11) demonstrates that at such high initial concentration of hydrogen hydride can form ahead of a crack tip at volume fractions almost close to 100%. Moreover, equilibrium of the hydride with local stress is reached in about 1 day. Fig. 12 shows the result of the large volume dilatation due to hydride formation on the normalized stress σ_{22}/σ_0. In the region ahead of the crack tip ($0 < R < 100$ μm, $\theta = 0$) stress is relaxed at equilibrium to values less than or equal to 50% of the stress for the hydrogen free material. However, the stress continues to be tensile due to the overriding effect of the applied loads.

5.3 Pressure tube outlet temperature ($T = 583$ K)

Fig. 13 shows the hydride volume fraction as a function of distance from the crack tip R at $\theta = 0$ for total elapsed times of 1 hour, 1 day, 1 month, 2 years and 25 years and an initial hydrogen concentration $c_0 = 0.01$ H/M (the stress free solvus was 0.0264 H/M). Equilibrium of the formed hydride with the applied stress is reached in less than a day, with 90% of the equilibrium volume fraction forming in about two hours. In this case hydride formation is essentially driven by the hydrostatic stress [Lufrano and Sofronis (1998)], and the effect of the deviatoric stress on the hydride zone shape is almost absent in contrast with the room temperature case (Fig. 5). This behavior can be attributed to the decreasing effect of the deviatoric stress on the mechanical energy of formation with temperature (Figs. 2-4) and the accompanying reduction of the yield stress. At room temperature and applied nondimensionalized hydrostatic stress of 2, the mechanical energy of formation is close to zero in the absence of any deviatoric effect (Fig. 2). In the presence of a nondimensionalized deviatoric stress of 1, the mechanical energy of formation reduces to -2.5 $kJ/mole$ (Fig. 2). At temperature 583 K, the mechanical energy of formation is just less than zero under pure nondimensionalized hydrostatic stress of 2 (Fig. 4). Addition of a nondimensionalized deviatoric stress of 1 reduces the mechanical energy of formation only by 1 $kJ/mole$ (Fig. 4). Fig. 14 shows the hydride volume dilatation effect on the relaxation of the stress σ_{22}/σ_0 ahead of the crack tip at $\theta = 0$. Clearly the effect is not as dramatic as in the case of 523 K and the same initial hydrogen concentration of 0.01 H/M (Fig. 12). At equilibrium, the stress peak is relaxed by $\sim$30% (Fig. 14) whereas the corresponding amount at 523 K is close to 60% (Fig. 12). This can be explained by comparing the hydride profiles of Fig. 11 and 13. At 523K, both the values of the hydride volume fraction and the size of the hydride zone ahead of the crack tip are greater than the corresponding values at 583 K. This derives from the fact that the solvus concentration at 583 K (Fig. 4) is greater than the solvus concentration at 523 K (Fig. 3) at a given combination of deviatoric and hydrostatic stress.

Lastly, the results of Figs. 12 and 14 on the hydride induced stress relaxation demonstrate that the mechanics problem is strongly coupled to the hydride precipitation especially at high temperatures and large initial concentrations. Moreover, the stress in the hydride ahead of the crack tip is tensile owing to

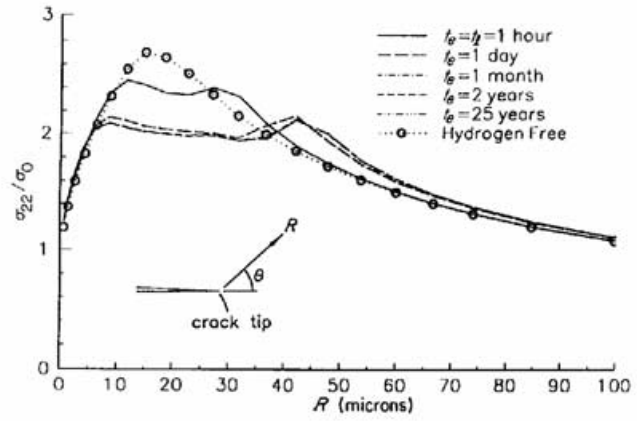

Figure 10 : Plot of the normalized normal stress σ_{22}/σ_0 versus distance R ahead of the crack tip at $\theta = 0$ after total elapsed times $t_e = 1$ hour, 1 day, 1 month, 2 years and 25 years. The load time was $t_l = 3600$, $K_A = 20\ MPa\sqrt{m}$, the initial concentration 0.003 H/M, and the temperature 523 K.

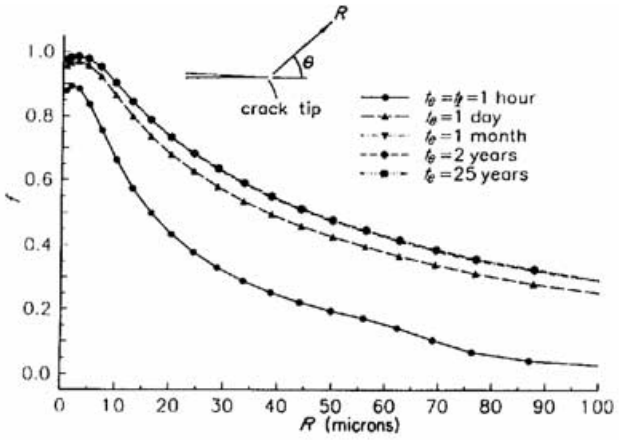

Figure 11 : Plot of the hydride volume fraction f versus distance R ahead of the crack tip at $\theta = 0$ after total elapsed times $t_e = 1$ hour, 1 day, 1 month, 2 years and 25 years. The load time was $t_l = 3600$ seconds, $K_A = 20\ MPa\sqrt{m}$, the initial concentration 0.01 H/M, and the temperature 523 K.

the overriding effect of the external tensile loads. The implications of this tensile stress on the hydride fracture are discussed in the next Section.

6 Hydride Cracking

As discussed by Lufrano, Sofronis, and Birnbaum (1998), cleavage of a hydride particle in front of the crack tip may be modeled by using a Griffith approach to the fracture event. A necessary relationship can be obtained between the length a of the hydride particle, the energy needed to create new surface in the hydride, and the normal stress σ_{22}, in order for the cleavage event to be energetically favorable. For the formation of a penny shaped crack, the expression for the stress is given by

$$\sigma_{22} = \left[\frac{2\gamma_s E}{\pi(1-\nu^2)a}\right]^{1/2}, \tag{21}$$

where γ_s is the surface energy of the hydride phase. The parameter γ_s was calculated from the relationship $2\gamma_s = G_{IC} = K_{IC}^2(1-\nu^2)/E$ in which $K_{IC} = 5\ MPa\sqrt{m}$ [Simpson and Puls (1979); Gahr, Makenas, and Birnbaum (1980)].

Since the transient stress field in front of a crack can be monitored at any time during or after the loading of the test sample, the value for the critical size, i.e. length, of a hydride particle for cleavage to occur can be calculated with

$$a_{\text{crit}} = \frac{2\gamma_s E}{\pi(1-\nu^2)\sigma_{22}^2} \tag{22}$$

Using the values of stress from the samples loaded at $T = 523$ K (Figs. 10 and 12 for initial concentrations respectively equal to 0.003 and 0.01 H/M), one can plot the critical hydride particle size in front of a crack tip at an applied load $K_A = 20\ MPa\sqrt{m}$ upon the completion of loading as a function of the distance from the crack tip at $\theta = 0$ (Fig. 15). Fig. 15 shows that for $c_0 = 0.003\ H/M$, if a hydride particle forms in the region from 10 to 30 microns in front of the crack tip and is over 2 microns in length, then the brittle fracture of that particle is energetically favorable. In the case of $c_0 = 0.01\ H/M$, the corresponding region is from 0 to 100 microns and the corresponding length is 7 microns. The sizes of the critical hydride length and especially of the region characterized by the critical hydride length ahead of the crack tip depend strongly on the initial hydrogen concentration which affects the amounts of the forming hydride volume fraction and in turn, the amounts of stress relaxation. The calculations indicate that a higher initial concentration yields a broader hydride zone with a critical hydride size. Once the hydride particle cleaves, either the main crack advances through the cleaved hydride or new hydride is formed at the new stress concentration regions around the cleaved hydride particle. The newly formed hydride may subsequently cleave, setting off a continuing process which may end in the failure of the specimen.

One shortcoming of the probabilistic modeling is that it does not deliver any information on the size of the hydride particles [Lufrano, Sofronis, and Birnbaum (1998)]. Thus, in lieu of experimental data on hydride particle size or a model to monitor the kinetics of individual hydride particle growth in front of the crack tip an averaging approach is used to estimate the hydride size directly ahead of the crack tip. Suppose that the region directly ahead of the crack tip along $\theta = 0$ has a hydride volume fraction distribution $f(R)$, where R is the dis-

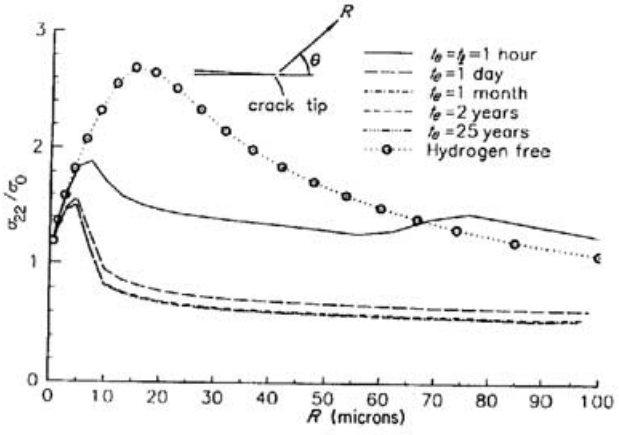

Figure 12 : Plot of the normalized normal stress σ_{22}/σ_0 versus distance R ahead of the crack tip at $\theta = 0$ after total elapsed times $t_e = 1$ hour, 1 day, 1 month, 2 years and 25 years. The load time was $t_l = 3600$, $K_A = 20\ MPa\sqrt{m}$, the initial concentration 0.01 H/M, and the temperature 523 K.

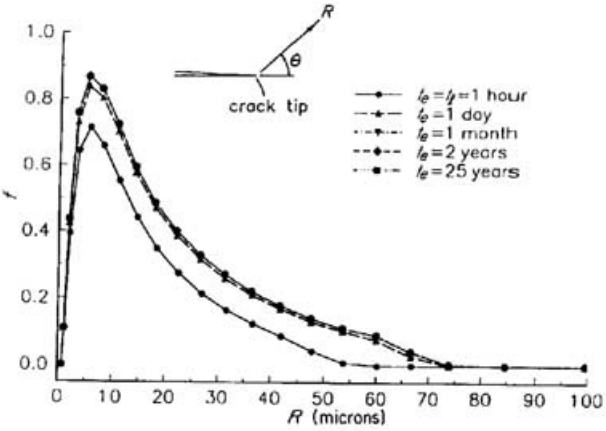

Figure 13 : Plot of the hydride volume fraction f versus distance R ahead of the crack tip at $\theta = 0$ after total elapsed times $t_e = 1$ hour, 1 day, 1 month, 2 years and 25 years. The load time was $t_l = 3600$ seconds, $K_A = 20\ MPa\sqrt{m}$, the initial concentration 0.01 H/M, and the temperature 583 K.

tance from the tip and $f = 0$ for $R > a_0$ (see inset of Fig. 16). It is reasonable to assume that an individual hydride particle in this region could be as large as $\overline{f}a_0$ in length, where $\overline{f}$ is the average hydride volume fraction in the region $0 < R < a_0$. With this method of estimation of the hydride particle size, it is possible to monitor the hydride growth in front of the crack along $\theta = 0$ and to predict at what time and load a hydride particle size will reach the critical hydride size as expressed by Eq. (22). In the numerical experiments, the level of the applied load is applied incrementally in a linear fashion until the fracture criterion is reached. Therefore, one may define the fracture toughness in the presence of hydrogen K_{IC} as the level of the applied load measured in terms of applied stress intensity factor K_A at the moment when the fracture criterion $a = a_{\text{crit}}$ is satisfied [Lufrano, Sofronis, and Birnbaum (1998)]. This is a conservative fracture toughness prediction since the presence of a void ahead of a blunting crack tip due to cracking of a hydride particle does not necessarily lead to fracture.

Fig. 16 shows the level of the applied stress intensity factor K_{IC} when the fracture criterion listed above was satisfied, for a test sample loaded at $T = 523\ K$ and rates of 0.02, 0.2, 2, 20, 200, 2000 $MPa\sqrt{m}/hr$. The fracture toughness K_{IC} is sensitive to the loading rate and the initial hydrogen concentration. Since the ability of diffusion to deliver hydrogen to the crack tip (thereby allowing the formation of hydride) is independent of stress as the loading rate increases, the amount of plasticity that precedes the formation of hydride with the critical size increases and hence the fracture toughness increases K_{IC} with the loading rate. The fracture toughness decreases with increasing initial hydrogen concentration because the average hydride volume fraction and hence the hydride particle size is larger (Fig. 9 and 11) at higher initial concentrations. Naturally, the fracture toughness K_{IC} of the material in the presence of hydrogen, as defined above, will also depend on the temperature.

7 Conclusions

Hydride formation at a blunting crack tip under plane strain tensile loading has been simulated in zircalloy. The model assumes elastoplastic accommodation of the forming hydride and is based on a purely dilatant transformation strain upon precipitation. The elastoplastic material response implies that the mechanical energy of formation and in turn, the solvus concentration also depend on the deviatoric stress in the matrix. The time required for equilibrium of the local hydride volume fraction to be reached with local stress varies from a few days, at the inlet tube temperature, to a few hours, at the outlet tube temperature. At room temperature, the time for equilibrium is calculated to be $\sim$2 years. In general, the time for equilibrium was found to be decreasing with increasing initial concentration at high temperatures, but no significant dependence was detected at room temperature. At all temperatures, substantial autocatalytic precipitation was observed after the loading was terminated and held fixed at its final value. On the basis of the Griffith fracture criterion, hydride formation was found to decrease the fracture toughness of zircalloy to levels close to those of the pure hydride phase. The final fracture toughness of the material was found to decrease with increasing initial hydrogen concentration and decreasing loading strain rate.

Acknowledgement: This work was supported by the

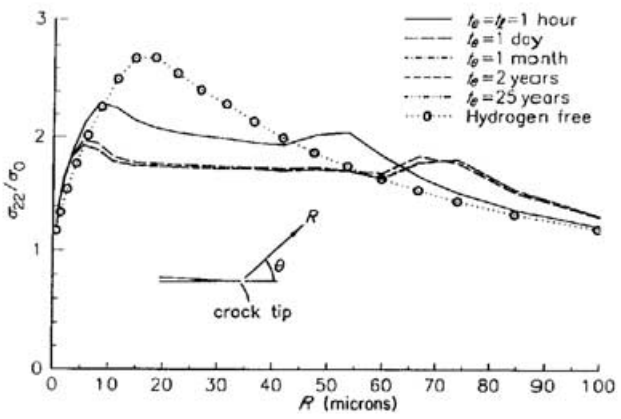

Figure 14 : Plot of the normalized normal stress σ_{22}/σ_0 versus distance R ahead of the crack tip at $\theta = 0$ after total elapsed times $t_e = 1$ hour, 1 day, 1 month, 2 years and 25 years. The load time was $t_l = 3600$, $K_A = 20\ MPa\sqrt{m}$, the initial concentration 0.01 H/M, and the temperature 583 K.

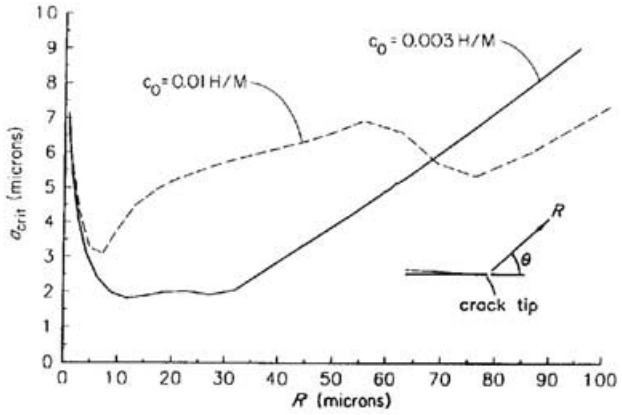

Figure 15 : Plot of the critical hydride particle size a_{crit} versus distance R ahead of the crack tip at $\theta = 0$ after the completion of loading ($K_A = 20\ MPa\sqrt{m}$) at time $t_l = 3600$ seconds for two different initial concentrations of hydrogen and temperature 523 K.

Atomic Energy Control Board of Canada under grant O66SS. 87055-5-5068 "Hydrogen related cracking in pressure tubes."

References

Birnbaum, H. K. (1984): Hydrogen related second phase embrittlement of solids. In Gibala, R.; Hehemann, R. F.(Eds): *Hydrogen Embrittlement and Stress Corrosion Cracking*, pp. 153–177, (Proceedings of a Troiano Festchrift Symposium, Case Western Reserve University, June 1-3, 1980).

Birnbaum, H. K. (1990): Mechanisms of hydrogen related fracture of metals. In Moody, N. R.; Thompson, A. W.(Eds): *Hydrogen Effects on Material behavior*, pp. 639–690, (Proceedings of the Fourth International Conference on the Effect of Hydrogen on the Behavior of Materials, Moran, Wyoming, September 12-15, 1989).

Birnbaum, H. K.; Grossbeck, M. L.; Amano, M. (1976): Hydride precipitation in nb and some properties of nbh. *J. Less Comm. Met.*, vol. 49, pp. 357–370.

Birnbaum, H. K.; Robertson, I. M.; Sofronis, P.; Teter, D. (1997): Mechanisms of hydrogen related fracture—a review. In Magnin, T.(Ed): *Corrosion Deformation Interactions CDI'96*, pp. 172–195, (Second International Conference, Nice, France, 1996).

Birnbaum, H. K.; Sofronis, P. (1994): Hydrogen-enhanced localized plasticity-a mechanism for hydrogen related fracture. *Mater. Sci. & Eng.*, vol. A176, pp. 191–202.

Dutton, R.; Nuttall, K.; Puls, M. P.; Simpson, L. A. (1977): Mechanisms of hydrogen induced delayed cracking in hydride forming materials. *Met Trans.*, vol. 8A, pp. 1553–1562.

Dutton, R.; Puls, M. P. (1976): A theoretical model for hydrogen induced subcritical crack growth. In Thompson, A. W.; Bernstein, I. M.(Eds): *Effect of Hydrogen Behavior of Materials*, pp. 516–525.

Earmme, Y. Y.; Johnson, W. C.; Lee, J. K. (1981): Plastic relaxation of the transformation strain energy of a misfitting spherical precipitate: linear and power law strain hardening. *Met Trans.*, vol. 12A, pp. 1521–1529.

Ellyin, F.; Wu, J. (1994): Effect of hydride precipitation on the elastoplastic stress field near a crack tip. *Acta Metall.*, vol. 42, pp. 2709–2717.

Eshelby, J. D. (1956): The continuum theory of lattice defects. In Seitz, F.; Turnbull, D.(Eds): *Solid State Physics*, volume 3, pp. 79–144. Academic Press, New York.

Eshelby, J. D. (1957): The determination of the elastic field of an ellipsoidal inclusion and related problems. *Proc. R. Soc.*, vol. A241, pp. 376–396.

Flannagan, T. B.; Mason, N. B.; Birnbaum, H. K. (1981): The effect of stress on hydride precipitation. *Scr. Met.*, vol. 15, pp. 109–112.

Gahr, S.; Birnbaum, H. K. (1978): Hydrogen embrittlement of nb iii - high temperature behavior. *Acta. Metall.*, vol. 26, pp. 1781–1788.

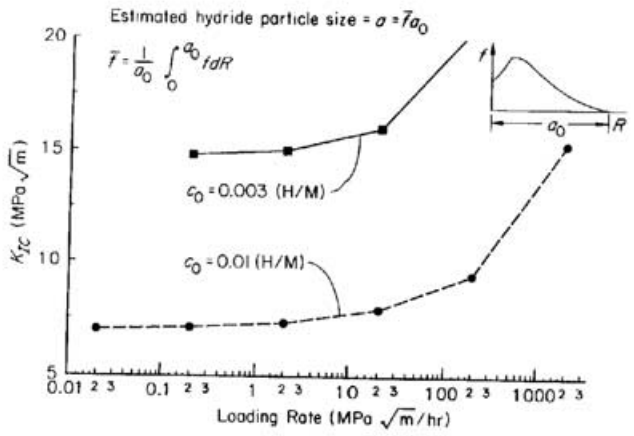

Figure 16 : Plot of the predicted fracture toughness K_{IC} versus the loading rate for two different initial concentrations of hydrogen and temperature 523 K.

Gahr, S.; Grossbeck, M. L.; Birnbaum, H. K. (1977): Hydrogen embrittlement of nb i - macroscopic behavior at low temperatures. *Acta Metall.*, vol. 25, pp. 125–134.

Gahr, S.; Makenas, B. J.; Birnbaum, H. K. (1980): Fracture of niobium hydrides. *Acta Metall.*, vol. 28, pp. 1207–1213.

Govindarajan, R. M.; Aravas, N. (1994): Deformation processing of metal powders: part i - cold isostatic pressing. *Int. J. Mech. Sci.*, vol. 36, pp. 343–357.

Grossbeck, M. L.; Birnbaum, H. K. (1977): Low temperature hydrogen embrittlement of niobium ii - microscopic observations. *Acta Metall.*, vol. 25, pp. 135–147.

Lee, J. K.; Earmme, Y. Y.; Aaronson, H. I.; Russell, K. C. (1980): Plastic relaxation of the transformation strain energy of a misfitting spherical precipitate: ideal plastic behavior. *Met Trans.*, vol. 11A, pp. 1837–1874.

Leitch, B. W.; Puls, M. P. (1992): Finite element calculations of the accommodation energy of a misfitting precipitate in an elastic-plastic matrix. *Met Trans.*, vol. 23A, pp. 797–806.

Lufrano, J. M. (1996): *Hydrogen transport in hydride and non-hydride forming metals and the mechanistic implications for fracture behavior*. Ph.D. Thesis, University of Illinois at Urbana-Champaign, Urbana, IL.

Lufrano, J. M.; Sofronis, P. (1998): *A solid mechanics approach to the modeling of hydride formation and cracking in zirconium alloys*. Report submitted to the Atomic Energy Control Board of Canada, Ottawa, Ontario.

Lufrano, J. M.; Sofronis, P.; Birnbaum, H. K. (1996): Modeling of hydrogen transport and elastically accommodated hydride formation near a crack tip. *J. Mech. Phys. Solids*, vol. 44, pp. 179–205.

Lufrano, J. M.; Sofronis, P.; Birnbaum, H. K. (1998): Elastoplastically accommodated hydride formation and embrittlement. *J. Mech. Phys. Solids*, vol. 46, pp. 1497–1520.

Makenas, B. J.; Birnbaum, H. K. (1980): Phase changes in the niobium- hydrogen system i: Accommodation effects during hydride precipitation. *Acta Metall.*, vol. 28, pp. 979–988.

McMeeking, R. M.; Rice, J. R. (1975): Finite-element formulations for problems of large elastic-plastic deformation. *Int. J. Solids Structures*, vol. 11, pp. 601–616.

Nagtegaal, J. C.; Parks, D. M.; Rice, J. R. (1974): On numerically accurate finite element solutions in the fully plastic range. *Comp. Meth. Appl. Mech. Eng.*, vol. 4, pp. 153–177.

Peisl, H. (1978): Lattice strains due to hydrogen in metals. In Alefeld, G.; Volkl, J.(Eds): *Hydrogen in Metals I, Topics in Applied Physics*, volume 28, pp. 53–74. Springer-Verlag, New York.

Puls, M. P. (1978): *Hydrogen induced delayed cracking: 1. strain energy effects on hydrogen solubility*. Atomic Energy of Canada Limited Report, AECL-6302, Pinawa, Manitoba.

Puls, M. P. (1981): The effects of misfit and external stresses on the terminal solid solubility in hydride-forming metals. *Acta Metall.*, vol. 29, pp. 1961–1968.

Puls, M. P. (1984): Elastic and plastic accommodation effects on metal-hydride solubility. *Acta Metall.*, vol. 32, pp. 1259–1269.

Puls, M. P. (1990): Effects of crack tip stress states and hydride-matrix interaction stresses on delayed hydride cracking. *Met. Trans.*, vol. 21A, pp. 2905–2917.

Shi, S.-Q.; Shek, G. K.; Puls, M. P. (1995): Hydrogen concentration limit and critical temperatures for delayed hydride cracking in zirconium alloys. *J. Nucl. Mater.*, vol. 218, pp. 189–201.

Shih, D. S.; Robertson, I. M.; Birnbaum, H. K. (1988): Hydrogen embrittlement of titanium: in situ tem studies. *Acta Metall*, vol. 36, pp. 111–124.

Simpson, L. A.; Puls, M. P. (1979): The effects of stress, temperature and hydrogen content on hydride-induced crack growth in Zr-2.5%nb. *Met. Trans.*, vol. 10A, pp. 1093–1105.

Sofronis, P.; McMeeking, R. M. (1989): Numerical analysis of hydrogen transport near a blunting crack tip. *J. Mech. Phys. Solids*, vol. 37, pp. 317–350.

Somenkov, V. A. (1972): Structure of hydrides. *Berichte Der Bunsen-Gesellschaft Fur Physikalische Chemie*, vol. 76, pp. 733–740.

Suzuki, T. (1985): Delocalization and superdiffusion of hydrogen isotopes in Va-metals. *Trans. J. Institute Metals*, vol. 26, pp. 601–614.

Takano, S.; Suzuki, T. (1974): An electron-optical study of -hydride and hydrogen embrittlement of vanadium. *Acta Metall.*, vol. 22, pp. 265–274.

Völkl, J.; Alefeld, G. (1978): Diffusion of hydrogen in metals. In Alefeld, G.; Volkl, J.(Eds): *Hydrogen in Metals I, Topics in Applied Physics*, volume 28, pp. 53–74. Springer-Verlag, New York.

Westlake, D. G. (1969): A generalized model for hydrogen embrittlement. *Trans. ASM*, vol. 62, pp. 1000–1006.